Habitable Planets with High Obliquities[1]

Darren M. Williams

Department of Astronomy and Astrophysics, Pennsylvania State University, 525 Davey Laboratory, University Park, Pennsylvania 16802
E-mail: dwilliams@astro.psu.edu

and

James F. Kasting

Department of Geosciences, Pennsylvania State University, 211 Deike Building, University Park, Pennsylvania 16802

Earth's obliquity would vary chaotically from 0° to 85° were it not for the presence of the Moon (J. Laskar, F. Joutel, and P. Robutel, 1993, *Nature* 361, 615–617). The Moon itself is thought to be an accident of accretion, formed by a glancing blow from a Mars-sized planetesimal. Hence, planets with similar moons and stable obliquities may be extremely rare. This has lead Laskar and colleagues to suggest that the number of Earth-like planets with high obliquities and temperate, life-supporting climates may be small.

To test this proposition, we have used an energy-balance climate model to simulate Earth's climate at obliquities up to 90°. We show that Earth's climate would become regionally severe in such circumstances, with large seasonal cycles and accompanying temperature extremes on middle- and high-latitude continents which might be damaging to many forms of life. The response of other, hypothetical, Earth-like planets to large obliquity fluctuations depends on their land–sea distribution and on their position within the habitable zone (HZ) around their star. Planets with several modest-sized continents or equatorial supercontinents are more climatically stable than those with polar supercontinents. Planets farther out in the HZ are less affected by high obliquities because their atmospheres should accumulate CO₂ in response to the carbonate–silicate cycle. Dense, CO₂-rich atmospheres transport heat very effectively and therefore limit the magnitude of both seasonal cycles and latitudinal temperature gradients. We conclude that a significant fraction of extrasolar Earth-like planets may still be habitable, even if they are subject to large obliquity fluctuations. © 1997 Academic Press

1. INTRODUCTION

The recent discoveries of extrasolar planets (e.g., Wolszczan 1994, Mayor and Queloz 1995, Marcy and Butler 1996,

Butler and Marcy 1996, Gatewood 1996, Butler *et al.* 1996, Cochran *et al.* 1996) have generated widespread anticipation of detecting an Earth-like planet around a nearby solar-type star. As of this writing, all of the companions found around Sun-like main-sequence stars are at least 1.5 times the mass of Saturn, and none of these objects orbit entirely within a circumstellar habitable zone, or HZ (Williams *et al.* 1997). We follow Kasting *et al.* (1993, henceforth KWR) in defining the HZ as the region around a star in which an Earth-like planet (of comparable mass and having an atmosphere containing N₂, H₂O, and CO₂) is climatically suited for surface-dwelling, water-dependent life. KWR conservatively estimated the Sun's HZ to be ~0.4 AU wide, comparable in width to the average spacing of terrestrial planets in the Solar System. The 4.5-byr continuously habitable zone (CHZ) is about half this width, based on the same conservative assumptions. If planets in other systems are spaced similarly to those in our own Solar System, the chances of finding one within another star's HZ are pretty good, perhaps approaching 100% for stars of $1M_\odot$ (Wetherill 1996).

Laskar and Robutel (1993) complicated the discussion of planetary habitability with their discovery that the obliquities of the terrestrial planets (including a hypothetical moon-less Earth) in the Solar System undergo large-amplitude, chaotic fluctuations on time scales of ~10 myr. The reasons for obliquity variations are well understood. A gravitational couple exerted by the Sun (and the Moon in the case of Earth) on a planet's equatorial bulge causes precession of the spin axis about the orbit normal, as well as nutation, which changes the obliquity. Gravitational interactions with other planets cause orbit normals themselves to nutate and precess about the normal to the Solar System's invariable plane (the plane defined by the combined angular momenta of all the planets). When the precessions of the spin axis and orbit axis come into resonance,

large and unpredictable excursions in obliquity occur. Resonances between spin axis precession and the rate of precession of perihelion in a planet's orbit can also be important. Both types of interactions are termed *secular resonances* because they involve motions that are averaged over many planetary orbits.

This behavior has been well studied in the case of Mars (e.g., Ward 1973, 1979, 1991) whose spin axis fluctuates between 15° and 35° with dominant periods of 0.12 and 1.2 myr. Mars' obliquity possibly reaches 45° or 50° if a spin–orbit resonance is encountered (Ward 1991, Touma and Wisdom 1993). Laskar and Robutel (1993) predict chaotic obliquity fluctuations for Mars in spin–orbit resonance in the range 0° to 60°. A companion paper (Laskar *et al.* 1993) showed that Earth's obliquity would vary even more radically (0° to 85°) were it not for the stabilizing presence of the Moon. Nearly two-thirds of Earth's couple on its oblate figure is contributed by the Moon, with the remainder contributed by the Sun. Consequently, Earth precesses faster than any of the other terrestrial planets, and so avoids the numerous secular resonances that exist at lower frequencies.

Ward (1974) was perhaps first to mention that Earth's obliquity would vary much more than it does today if the Moon were not present. Although the variation found by Ward for a moon-less Earth was relatively small (±10°), he recognized that larger hypothetical variations would profoundly affect climate. For example, if Earth's obliquity ever exceeded 54°, the planet would receive more annual-average insolation at the poles than at the equator. Seasonal cycles at high latitudes would also become very pronounced when a planet's obliquity is high. The discovery that Earth might possibly reach an obliquity as high as 85° led Laskar *et al.* (1993) to suggest (albeit implicitly) that accompanying changes to climate might render Earth uninhabitable. The number of habitable planets around other stars may, therefore, be proportional to the fraction of planets with sizable moons. Earth's moon is currently thought to have been formed as a result of a glancing collision with a Mars-sized object during the latter stages of accretion (Hartmann *et al.* 1986). Such moon-forming collisions may be relatively improbable events; Earth is the only terrestrial planet with a large moon. If most Earth-sized planets lack large moons, and if the climatic excursions caused by the obliquity variations are too severe, the chances of finding life elsewhere in the galaxy may be significantly reduced.

We have used a one-dimensional (1-D) energy-balance climate model to investigate the effects of large obliquity fluctuations on climate and to formulate a reply to Laskar and colleagues' suggestion. Early versions of the model (Williams *et al.* 1996) gave surprisingly pessimistic results: monstrous seasonal cycles for planets with high obliquities yielded opposing solstice temperatures of 220 and 430 K

on high-latitude continents. Here, we show that an Earth-like planet can have its seasonal cycles damped and equator-to-pole temperature gradient reduced, provided it possesses a dense CO_2 atmosphere built up in response to the carbonate–silicate cycle. Such an atmosphere is expected to exist on planets located toward the outer edge of the HZ. Weathering on tectonically active planets enforces a balanced exchange of CO_2 between the atmosphere and the carbonate rock reservoir within the crust. Less than ~0.001% of Earth's 60-bar subsurface CO_2 inventory resides in the atmosphere; however, Earth-like planets within the outer HZ (1.1–1.4 AU) might lose more than 2% of their crustal carbonate in forming CO_2-rich atmospheres, provided they demonstrate similar amounts of volcanic activity. Many of these planets could have relatively stable climates even if they were subject to large obliquity variations. By demonstrating this explicitly, we show that obliquity variations are not an insurmountable obstacle to finding life around other stars.

2. MODEL DESCRIPTION

A. Energy-Balance Methods

The model employed for this study is a zonally averaged energy-balance climate model (EBCM), of the kind described in detail by North and Coakley (1979) and North *et al.* (1981) (see also Caldeira and Kasting 1992).

The operating principle of EBCMs is straightforward: planets in thermal equilibrium must on average radiate as much long-wave energy to space as they receive at UV, visible, and near-IR wavelengths from stars. Radiative energy fluxes entering or leaving a particular region are balanced by dynamic fluxes of heat transported into or away from the region by winds. Our model divides Earth into 18 latitudinal zones, each 10° wide. We express radiative and dynamic energy balance for each zone by

$$C \frac{\partial T(x,t)}{\partial t} - \frac{\partial}{\partial x} D(1-x^2) \frac{\partial T(x,t)}{\partial x} + I = S(1-A), \quad (1)$$

where x is the sine of latitude and T is the zonally averaged surface temperature. The terms in the energy-balance equation represent, from right to left, the absorbed fraction of incident solar flux, S, where A is the top-of-atmosphere albedo; outgoing infrared flux to space, I; latitudinal heat transport (modeled as diffusion); and the rate of seasonal heating and cooling. The thermal inertia is determined by the effective heat capacity, C, of the surface ocean and atmosphere. The diffusion coefficient, D, is a measure of the transport efficiency, which is assumed to depend on atmospheric pressure (see Section 2C).

We used a 1-D radiative–convective model (Kasting and Ackerman 1986, Kasting 1988, 1991) to parameterize top-

of-atmosphere albedo as a function of surface temperature, CO_2 partial pressure, solar zenith angle, and surface albedo. For these calculations, the atmosphere was assumed to consist of 1.0 bar N_2 and variable amounts of CO_2 and H_2O. The stratosphere was assumed to be isothermal, following Kasting (1991), and the troposphere was assumed to be fully saturated with water vapor. Using a more realistic (for present Earth) distribution of relative humidity would have complicated the model without changing any of our basic conclusions.

Top-of-atmosphere albedo depends implicitly on temperature through its effect on the concentration of tropospheric water vapor, which reduces albedo by absorbing incoming solar energy in the near IR. We chose to exclude O_2 from the calculations because we wanted to give equal consideration to planets without photosynthetic life from which Earth's present oxygen level is derived. Again, the model results are only weakly sensitive to this assumption. CO_2 affects the albedo primarily through its contribution to Rayleigh scattering, which is important for the dense atmospheres encountered here.

All of the planets that we considered have Earth-like (30:70) land–sea ratios, and their geography is similar to Earth's unless otherwise indicated. Each latitudinal zone was partitioned between three surfaces: land, ocean, and sea-ice. The zone fraction covered by ocean was assigned a surface albedo that depends on solar zenith angle through the Fresnel reflectance formulas for water (see Appendix). Other surfaces were assigned albedos consistent with observations (Kondrat'ev 1969) and by making assumptions about snow cover. To keep the model simple, we have not attempted to simulate snowfall or the growth and decay of ice sheets. Rather, we simply assumed that snow is present on land surfaces at temperatures below 273 K, that its albedo diminishes with increasing temperature (Kondrat'ev 1969), that ice begins to form in the ocean below 273 K, and that the ocean fraction covered by ice also depends inversely on surface temperatures.

The radiative effects of H_2O clouds on climate are to raise the albedo and reduce the outgoing IR flux. We approximated Earth to be 50% overcast at any given moment, and we assumed that this fraction remains constant over a wide range of obliquities and orbital distances. Improving on this assumption would require a climate model much more sophisticated than the one we have developed, and even then one might not get the answer right. Our parameterization of short-wave cloud albedo was chosen to reproduce Earth's known latitudinal distribution of albedo (see Appendix).

Thermal inertia over the continents is determined by the heat capacity and IR opacity of the atmosphere. Oceanic areas contribute additional inertia from that heat capacity of the wind-mixed oceanic layer. We used a wind-mixed oceanic layer depth of 50 m and assigned intermediate heat capacities to the atmosphere over sea-ice and over the ice caps, to best reproduce Earth's seasonal cycles.

B. The Carbonate–Silicate Cycle

A key aspect of our attempt to simulate climate on planets with orbital characteristics and obliquities far removed from Earth's was to include the carbonate–silicate cycle, which controls the concentration of atmospheric CO_2 and, thus, the magnitude of the greenhouse effect. In this cycle, CO_2 released from volcanos is consumed by weathering of silicate minerals and precipitation of carbonate sediments on the sea floor. The rates of these processes on Earth must balance on time scales in excess of a half-million years (see Holland 1978, Berner *et al.* 1983). The negative feedback that keeps the cycle in balance involves the dependence of silicate weathering rate on temperature (Walker *et al.* 1981). If surface temperatures become too low, silicate weathering slows down, and volcanic CO_2 accumulates in the atmosphere until the surface warms up. Conversely, if the surface temperature is too high, silicate weathering speeds up, CO_2 is removed from the atmosphere, the greenhouse effect diminishes, and the surface cools down.

Weathering was parameterized in the model as a function of zonal temperature and the available weathering surface, which is the zonal land fraction with $T > 273$ K. We adopted the weathering dependence on temperature suggested by Berner *et al.* (1983),

$$
\begin{aligned}
W(T) = [1 &+ 0.087(T - T_0) \\
&+ 1.86 \times 10^{-3}(T - T_0)^2]W_0,
\end{aligned}
\tag{2}
$$

where T is the zonally averaged surface temperature, T_0 is taken to be the planet average temperature (288 K) of present Earth, and W_0 is the present rate of CO_2 consumption by silicate weathering, 3.3×10^{14} g year^{-1} (Holland 1978). Averaged over all latitude belts and over the seasonal cycle, the mean weathering rate, $\overline{W}$, must equal the estimated global CO_2 production by volcanos, which is assumed to be equal to W_0. This balance may be written as

$$
\overline{W} = \frac{C_w \int_0^\tau dt \sum_{n=1}^{n\,\text{belts}} A_n[1 + 0.087(T_n - T_0) + 1.86 \times 10^{-3}(T_n - T_0)^2]}{\int_0^\tau dt},
\tag{3}
$$

where A_n is the fractional zonal area available for weathering, $\tau = 1$ year, and $C_w = 2.88$ is a constant which we adjusted to balance global weathering and outgassing for present Earth. The additional constant is required because our time- and spatially varying weathering rate does not

equal the weathering rate calculated at a fixed global-mean surface temperature.

In our parameterization, the globally and annually averaged silicate weathering rate is always assumed to be equal to the volcanic outgassing rate of CO_2 on the present Earth. This implies that a planet that receives less sunlight than does Earth must have a higher atmospheric CO_2 concentration. Thus, planets farther out in the HZ tend to accumulate dense, CO_2-rich atmospheres. [The terrestrial planets do not follow this pattern, but that is because Venus is inside the inner edge of the HZ (Kasting 1988), and Mars is too small to recycle CO_2 effectively (Pollack *et al.* 1987).] Atmospheric CO_2 levels can also change in our model if the planetary obliquity is varied or if the surface geography is changed, because both of these factors affect the weathering rates calculated by Eq. (3).

Note that our model assumes that atmospheric CO_2 levels respond instantly to changes in planetary obliquity. This is a reasonable assumption for a planet with Earth's CO_2 concentration, because the time scale for the carbonate–silicate cycle to equilibrate (~0.5 myr) is shorter than the 10-myr time scale for large, chaotic obliquity fluctuations (Laskar and Robutel 1993); however, atmospheric CO_2 would not have time to equilibrate over the 41,000-year period of Earth's current obliquity variation or over the shorter (120,000-year) of the two dominant periods over which Mars' obliquity varies. So, the obliquities assumed in our climate simulations may be thought of as the average over one of these short-term cycles.

C. Dynamic Heat Transport

Transport of heat by advection is critical to the zonal energy balance of planets with high obliquities because their atmospheres develop large temperature gradients which should drive the winds. Traditional treatment of dynamic heat transport in EBCMs has been to average the velocity field over a scale height and around the planet and to model the heat flow as diffusion using the transport term of Eq. (1). The diffusion coefficient, D, is commonly adjusted until models comfortably reproduce Earth's present latitudinal temperature gradient (see North *et al.* 1981). Some investigators (Lindzen and Farrell 1977) have attempted a more realistic representation of transport by parameterizing D as a function of latitude, allowing for the differences in transport efficiency between the symmetric Hadley regime below 30° latitude to a baroclinic eddy transport regime at midlatitudes. Here we have employed a methodology similar to that of Hoffert *et al.* (1981), who parameterized transport efficiency as a function of dynamic factors which may vary greatly from one atmosphere to another.

The case of Venus suggests that atmospheric pressure and planetary rotation rate are important transport param-

eters. Venus' atmosphere is ~100 times more massive than Earth's and exhibits an extensive Hadley circulation that heats the poles to within a few degrees of the equatorial temperature (Schubert 1983). A measure of the efficiency and poleward extent of the Hadley circulation is the Rossby number, R, expressed by Farrell (1990) as

$$R = gH\delta_h/\Omega^2 r^2, \tag{4}$$

where g is gravitational acceleration, r is planet radius, H is pressure scale height, Ω is planet rotation rate, and δ_h is latitudinal temperature gradient.

The Rossby number for Earth is ~0.2, which corresponds to a Hadley cutoff latitude of ~30° (Farrell 1990). The Rossby parameter for Venus is ~10^4 times that of Earth, allowing its Hadley circulation to reach the pole. An examination of the Rossby number form, however, reveals no explicit atmospheric pressure dependence, indicating that the strength of Hadley transport on Venus derives not so much from its dense atmosphere as it does from its slow rotation ($2\pi/\Omega = 243$ days). Hadley circulation is truncated at midlatitudes on rapidly rotating planets (e.g., Earth) by large Coriolis forces that deflect air masses azimuthally and disrupt the symmetry of the north–south flow.

Neither Venus nor Earth rotates at its primordial rotation rate, as they have been affected by tidal interactions with the Sun and Moon, respectively (Laskar and Robutel 1993); however, the 24-hr rotation rate of Mars suggests that terrestrial planets born and evolving in relative tidal isolation will have rotation periods of many hours rather than many days. For want of a better choice, the planets we consider here are assumed to have 24-hr rotation periods, which implies that the extent of their Hadley circulations should be similar to Earth's.

Changes to scale height, $H = RT/mg$, will also affect Hadley heat transport. Temperatures do not vary much in the model atmospheres considered here, but the mean molecular weight, m, increases as the atmospheres become more CO_2-rich. All else being equal, larger mean molecular weights for atmospheres of planets in the outer HZ (assuming N_2 is the other dominant gas) will cause the extent of their Hadley circulations to be slightly smaller.

The above discussion implies that dynamic heat transport on rapidly rotating, Earth-like planets will be accomplished most effectively by baroclinic eddies. The dynamical heat flux, Q_d, caused by eddy circulation is expressed by Gierasch and Toon (1973) as the following proportionality:

$$Q_d \propto \int_0^\infty \rho c_p \overline{vT} \, dz. \tag{5}$$

The velocity, v, and temperature, T, of the flow are averaged over longitude and time, ρ is the density, c_p is the

heat capacity of the atmosphere, and the integral is carried over height, z. Using the hydrostatic law and assuming $\overline{vT}$ varies little with height, Eq. (5) may be written

$$Q_d \propto p c_p \overline{vT}, \tag{6}$$

giving the desired transport dependence on atmospheric pressure p. Additional dependences can be inferred by examining the form of $\overline{vT}$ given by Stone (1972),

$$\overline{vT} \propto \frac{1}{m^2 f^2}, \tag{7}$$

where f is the Coriolis parameter, $\propto \Omega$. It is comforting to recognize that these variables are components of the Rossby number considered previously, and additionally that the dominant rotation dependence (Ω^{-2}) is common to both forms. A notable difference is the m^{-2} dependence here compared with the m^{-1} dependence in the Rossby number. For consistency, we have included the dependence of transport on heat capacity, c_p, which is slightly lower (14%) for CO_2 than for N_2. Combining Eqs. (5) and (6), we obtain

$$Q_d \propto p c_p m^{-2} \Omega^{-2}. \tag{8}$$

The constant for proportionality, D, may be expressed in terms of normalized variables (with the subscript 0 referring to present Earth) as

$$\left(\frac{D}{D_0}\right) = \left(\frac{p}{p_0}\right)\left(\frac{c_p}{c_{p_0}}\right)\left(\frac{m_0}{m}\right)^2 \left(\frac{\Omega_0}{\Omega}\right)^2. \tag{9}$$

We adjusted $D_0 = 0.58 \ \mathrm{W \ m^{-2} \ K^{-1}}$ to match Earth's present latitudinal temperature gradient, and the latitude ($\sim72°$) of the 263 K seasonal-mean ice line. We took $c_{p_0} = 1.0 \times 10^3 \ \mathrm{g^{-1} \ K^{-1}}$ (*CRC Handbook of Chemistry and Physics, 1985–1986 Edition*), $m_0 = 28.0$, and $\Omega = \Omega_0 = 7.27 \times 10^{-5}$ rad sec^{-1}.

D. CO_2 Clouds

The HZ outer edge has been suggested by KWR to be the distance at which CO_2 first condenses to form clouds within a planet's atmosphere. This is clearly a conservative assumption, as CO_2 clouds should not noticeably affect climate until they begin forming over large portions of the planet, and because high-altitude CO_2 clouds may warm, rather than cool (as do cirrus clouds on Earth). KWR could not look at the spatial and temporal distribution of CO_2 clouds because their model was one dimensional and time independent. We revisited this problem with the energy-balance model to determine where and when clouds form

TABLE I
Model Output with Earth at 1.0 AU

geography	obl. (°)	T_{av} (K)	A_{av}	pCO_2 (ppm)	T_{max} (K)		T_{min} (K)	
present	23.5	288.1	0.311	330.	304.5	(-5°)	241.3	(85°)
equatorial	.	276.6	0.351	44.0	293.3	(-5°)	234.6	(-85°)
polar	.	282.4	0.323	38.7	325.9	(-85°)	217.0	(-85°)
polar	35.0	250.0	0.510	11.8	364.0	(-85°)	195.7	(-85°)
present	90.0	282.3	0.312	19.4	352.2	(-85°)	266.4	(15°)
equatorial	.	300.2	0.269	1670	339.4	(-85°)	274.1	(-5°)

Note: obl is obliquity, T_{av} is the seasonal- and global-mean temperature, A_{av} is the seasonal- and global-mean albedo, and pCO_2 is carbon dioxide partial pressure, given in parts per million. Global temperature extremes, T_{max} and T_{min}, are listed left of the latitudes at which they occur.

and to provide a revised estimate for the HZ outer edge. The troposphere in each latitude zone was searched seasonally for clouds by comparing the saturation vapor pressure of CO_2 to its ambient pressure using the method outlined in the Appendix. As in KWR, CO_2 clouds were not included explictly in the planetary radiation balance. Only their effect on the tropospheric lapse rate was taken into account.

3. RESULTS

A. Earth's Present Climate

First, we adjusted the model's free parameters to obtain a reasonable approximation of Earth's climate at 23.5° obliquity. We payed particularly close attention to reproducing the seasonal- and global-mean albedo (0.31) and surface temperature (288 K), the latitude of the permanent ice line (72°), and the amplitudes of zonal seasonal cycles. Results of the modeling are given in Table I and Fig. 1A, where we illustrate how zonal temperatures vary over a 1-year seasonal cycle.

Focusing our attention on the zone centered on +45°, we find that the temperature varies from 271.3 K (−1.8°C) to 285.8 K (12.7°C) with a seasonal cycle amplitude of 7.3 K, which is substantially smaller than the observed amplitude (~16°C) for continental interiors at this latitude on Earth. Thus, our model amplitudes in zones containing substantial amounts of water are less than half the size of observed amplitudes over continents in the same zone, in good agreement with seasonal cycle amplitude differences found using a more sophisticated 2-D model (North *et al.* 1983) that resolved the continents and oceans.

Our simpler model averages the heat capacities for land and ocean within a zone around the entire globe. This presents the following problem: Because the model heat capacity for unfrozen ocean is 40 times that of the atmosphere over land, a simple weighting of the heat capacities by the respective zonal surface fractions yields a heat capacity characteristic of an oceanic zone rather than a continental zone. For zones with comparable amounts of land
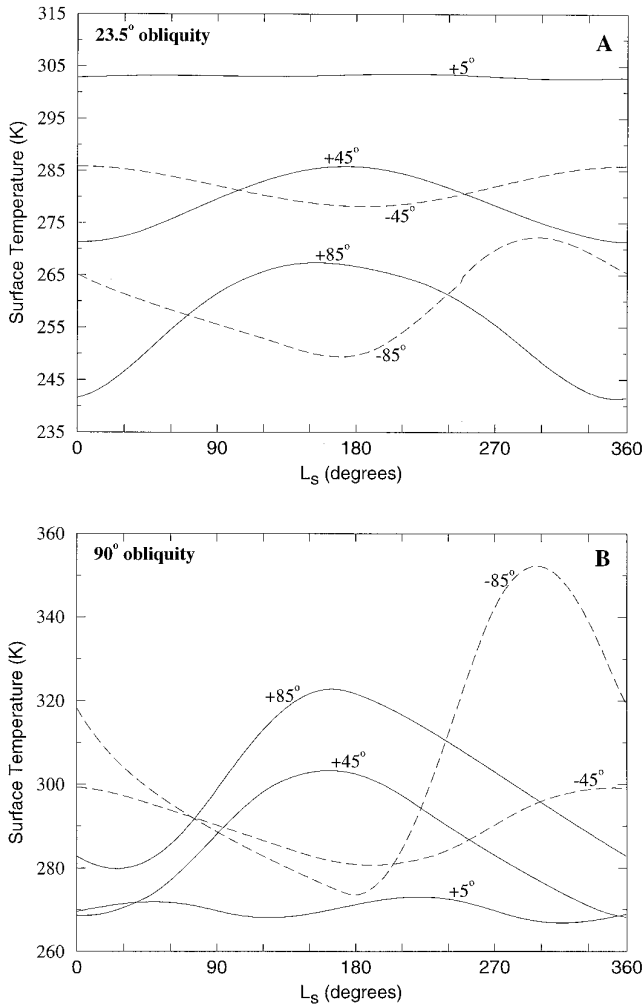
FIG. 1. Representative seasonal temperature cycles for Earth at (A) 23.5° obliquity and (B) 90° obliquity. L_s is the orbital longitude of the planet with respect to the vernal equinox ($L_s = 0°$ or 360°). Solstices occur at $L_s = 90°$ and 270°. Temperatures are shown for five latitude zones, each 10° wide and centered on the latitude labeling the curves. Northern latitudes are indicated by solid lines, and southern latitudes are indicated by dashed lines.

and sea (e.g., +45°), the zonally averaged heat capacity and, hence, thermal time scale are more than 20 times that over a continent. Thus, the magnitudes of temperature extremes returned by the model are substantially smaller than those that would occur over a continental interior.
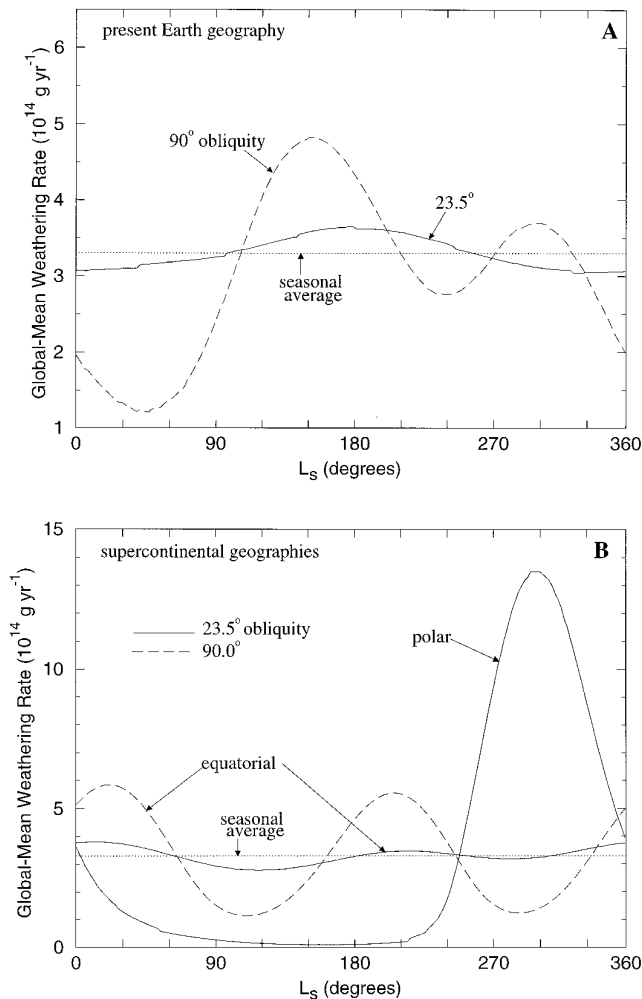
B. Earth at 90° Obliquity

Our second climate simulation was performed with Earth's obliquity set equal to 90°. Results for the run are given in Table I, and Fig. 1B illustrates the remarkable changes to Earth's climate that would follow. First, the tropics would become cold enough to sustain permanent snow cover because at high obliquity the Sun spends com-

paratively little time near the zenith at low latitudes. Also, each pole would be heated for 6 months, as they are at 23.5° obliquity, but with the Sun spending more than 40 days within 20° of polar zenith. Because the opposite period of cooling would be equivalent to the length of darkness experienced by the pole at any obliquity, the net change to polar climate would be a warming, which would cause the ice to melt.

In these circumstances, Earth's oceanic (northern) and continental (southern) poles would demonstrate markedly different seasonal cycle amplitudes because of their different thermal inertias. Despite the relatively high thermal inertia of the northern pole, the intensity and duration of sunlight experienced there at high obliquity doubles the amplitude of its temperature cycle (Fig. 1), bringing summer temperatures over the Arctic Ocean above 320 K. The seasonal variation in temperature over the southern pole is even more dramatic, with summer temperatures reaching 353 K, slightly lower than the survivable high-temperature limit (383 K) for thermophilic bacteria (Segerer *et al.* 1993), but higher than the maximum temperatures at which more advanced life forms survive today (~330 K). The seasonal minimum temperatures still dip below the freezing point of water.

Large seasonal temperature variations might also present a problem for life at lower latitudes. At +45°, for example, model temperatures are found to vary between 268 and 304 K. Over the continents at this latitude, the seasonal temperature variation could be twice this large, which would allow summertime temperatures to exceed 322 K and wintertime temperatures to fall below 250 K. Even more remarkable is that this variation, which exceeds the present range of temperatures observed on Earth today, would take place in only 6 months time. Whether any of Earth's dominant species could survive these rapid and large variations in temperature is an interesting biological question. Photosynthetic life might be substantially challenged by long (~90-day) periods of darkness during the winter at this latitude. Areas nearer the equator would have smaller seasonal temperature variations and shorter periods of darkness, however, so at least some areas of the planet might still be suitable for life at 90° obliquity.

Earth's CO_2 level would also be affected by its obliquity because the weathering rate depends on surface temperatures through Eq. (2). Figure 2A compares the seasonally varying global weathering rate for Earth at 23.5° and 90° obliquity. We find, in both cases, that the greatest weathering takes place during northern hemisphere summer, when the bulk of Earth's continents is warmest. Also, the weathering cycle amplitude is greater at high obliquity because the seasonal temperature variations are exaggerated. A second peak in the 90° obliquity weathering cycle results from weathering of continents in the southern hemisphere

FIG. 2. Variations in the global-mean weathering rate over a seasonal cycle for Earth at 1.0 AU and with 23.5° (solid lines) and 90° (dashed lines) obliquity. Cycles are shown for Earth with (A) present geography, and (B) two alternate geographies: a supercontinent covering 30% of Earth's surface centered on the equator, and a supercontinent centered on the south pole. The model forces the seasonal-average weathering rate to equal the CO_2 volcanic outgassing rate $= 3.3 \times 10^{14}$ g year^{-1} (dotted line).

around the winter solstice. Earth's equilibrium CO_2 level at 90° obliquity is 19.4 ppm (Table I), significantly lower than at present (330 ppm). This is because for a given CO_2 level, the continents weather more rapidly, on average, at 90° obliquity than at 23.5°. Thus, pCO_2 must equilibrate at a lower value for the high-obliquity planet than it does for the present Earth.

## C. Effects of Changing the Geography

The difference in seasonal cycle amplitude over the northern and southern poles in Fig. 1B shows the model to be very sensitive to the location of continents. The

difference would be even more pronounced if the Antarctic continent were larger because it would be able to sustain an even greater temperature gradient.

To examine the effects of continental size and position on climate for planets with different obliquities, we imitated Marshall et al. (1988) by performing simulations with all of Earth's continents clustered together to form a supercontinent, which we chose to center either on the equator or over the southern pole.

Results of our simulations are given in Table I and Fig. 2B. At 23.5° obliquity, an equatorial supercontinent would experience substantial weathering at the equinoxes. This would, in turn, draw down atmospheric CO_2 from 330 to 44 ppm, where the surface could cool enough to weather more slowly. Thus, the lower CO_2 level would safeguard the equatorial supercontinent from temperatures that might otherwise be warmer than Earth's tropics today. While permanent sea-ice caps would cover both poles poleward of ±52°, continental temperatures would range from 286 K to a mild 293 K, which would provide optimal conditions for terrestrial-type life.

At high obliquity, the equatorial supercontinent would cool initially, causing weathering to slow or even cease, and CO_2 would accumulate in the atmosphere. We find that 1670 ppm of CO_2 is needed to thaw the continent and raise the weathering rate. As at low obliquity, the greatest weathering takes place near the equinoxes when the continent is warmest. Even in this extreme case, the supercontinent would remain unfrozen with temperatures never falling below 274 K. The case of the polar supercontinent is more problematic because, even at 23.5° obliquity, areas near the southern pole would alternate between super-heated (326 K) and subpolar (217 K) states every 6 months. Only a narrow region near the coast of the supercontinent (−26° latitude) would demonstrate a seasonal cycle amplitude smaller than 30 K. Although the solar zenith angle would remain small during the sunlit summer months the prolonged illumination would be enough to warm the supercontinent and cause it to weather rapidly, as shown in Fig. 2B. Table I shows that the CO_2 level needed to balance the carbonate–silicate cycle (38.7 ppm) is even lower than for the case of the equatorial supercontinent. A slightly higher obliquity (35°) yields an even larger seasonal cycle and temperature extremes near the confidence limits (360 and 190 K, as set by the fits to top-of-atmosphere albedo (see Appendix)) of the model. For this case, an ice cap would cover the entire hemisphere opposite the continent, while the temperature extremes on the supercontinent would be everywhere damaging to life. These problems would be even more pronounced for planets having higher obliquities or for planets with smaller endowments of water and larger continents. Clearly, high-obliquity planets with polar supercontinents are not very attractive candidates for harboring land-based life.
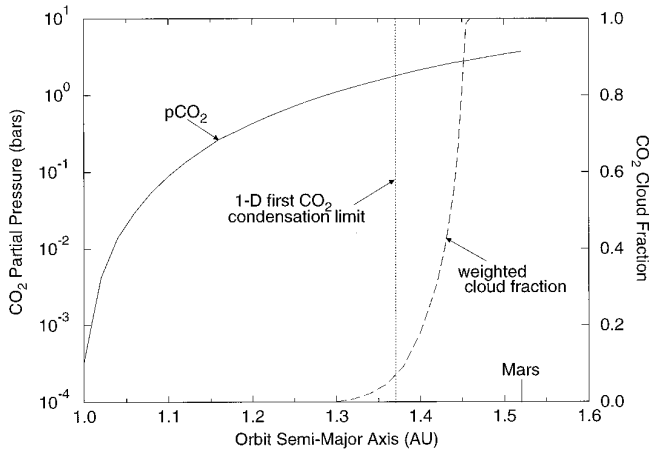
FIG. 3. Carbonate–silicate cycle equilibrium CO_2 levels (solid line) for Earth at a variety of positions within the HZ. The one-dimensional first-CO_2-condensation limit at 1.37 AU (dotted line) was found by KWR. CO_2 cloud fraction (dashed line) is an area- and insolation-weighted sum of the latitude zones in which clouds form somewhere within the troposphere.

D. Dense CO_2 Atmospheres and the HZ Outer Edge

Earth could circumvent the problems it would face at high obliquity or with a polar supercontinent if it were farther from the Sun, where its atmosphere might contain larger amounts of CO_2. A CO_2-rich atmosphere would have a long radiative time constant because CO_2 is highly opaque to infrared radiation leaving the planet. The increase in Earth's global thermal inertia would decrease the amplitude of its seasonal cycle and cause the climate to be only weakly sensitive to continental topography.

To determine how dense of an atmosphere one might expect to form, we performed simulations with Earth at several orbital positions between 1.0 and 1.5 AU, while holding its obliquity and geography constant at present values. The object was to determine the level of CO_2 required to balance the carbonate–silicate cycle at these distances. The results of these calculations are shown in Fig. 3. Steady-state atmospheric CO_2 partial pressures range from 3.3×10^{-4} bar for Earth in its present orbit to nearly 4.0 bars at 1.50 AU. The CO_2 partial pressure asymptotically approaches 5 bars at the "maximum greenhouse" limit of 1.67 AU, beyond which a planet cannot be warmed by further addition of CO_2 (KWR). Here, the increased albedo caused by CO_2 outweighs its contribution to greenhouse warming.

It is unlikely that a planet could remain habitable out to this distance, however, because the planet would be covered by CO_2 clouds. If these clouds extended down toward the surface, as they would near the maximum greenhouse limit, their radiative effect would almost certainly be to cool the planet. The distance at which CO_2

first condenses in a 1-D atmosphere was determined by KWR to be 1.37 AU (Fig. 3). This served as their conservative estimate of the HZ outer edge. Our two-dimensional model demonstrates that clouds first appear at the poles around 1.30 AU, and that they become widespread between 1.40 and 1.45 AU. Thus, a conservative choice for the outer edge of the Sun's present HZ is ~1.40 AU, not far from the 1-D estimate.

E. Temperature Gradients and Seasonal Cycles at 1.4 AU

Planets near the outer edge of the HZ have dense CO_2 atmospheres as a result of the carbonate–silicate cycle. One consequence of this is a reduction in the equator-to-pole temperature gradient. The reason for this reduction is twofold. First, the poles are not able to cool as rapidly in winter as they do beneath a relatively IR-transparent atmosphere at 1.0 AU. This results in a warming of the poles relative to the equator and a flattening of the latitudinal temperature profile (Fig. 4). The tropics are also warmed initially, but in these circumstances, the globally averaged surface temperature is too high to maintain the present global weathering rate. To compensate, the model adjusts (lowers) the concentration of CO_2 until temperatures are globally reduced (i.e., the temperature profile of Fig. 4 is lowered) and the global weathering rate is reequilibrated with the rate of CO_2 production by outgassing for the new latitudinal distribution of surface temperatures. Thus, despite its possessing a dense CO_2-rich atmosphere, Earth at 1.4 AU is shown to be cooler in the
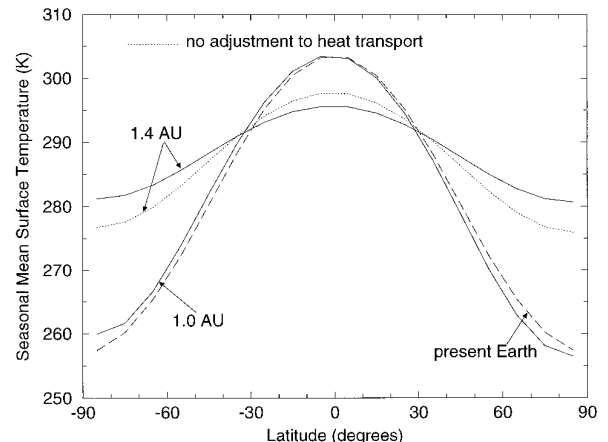
FIG. 4. Latitudinal temperature profiles for Earth at 1.0 and 1.4 AU (both marked with solid lines). The profile indicated by a dotted line is for Earth at 1.4 AU, with the heat transport parameter held constant ($D = 0.58$ W m^{-2} K^{-1}). Observations (dashed line) are taken from North and Coakley (1979) and parameterized as $T(x) = 14.2 - 30.2 P_2(x)$, where T is the seasonal-average surface temperature (°C), x is the sine of latitude, and $P_2(x)$ is the second Legendre polynomial $(3x^2 - 1)/2$.

TABLE II
Model Output with Earth at 1.4 AU

geography	obl. (°)	T_{av} (K)	A_{av}	pCO_2 (bars)	T_{max} (K)		T_{min} (K)	
present	23.5	290.6	0.337	2.12	296.4	(-15°)	274.5	(85°)
equatorial	.	285.5	0.346	1.89	291.5	(-5°)	272.4	(-85°)
polar	.	289.6	0.334	2.04	309.3	(-85°)	257.1	(-85°)
polar	65.0	246.2	0.488	1.15	362.8	(-85°)	189.9	(-85°)
present	90.0	287.9	0.324	1.87	319.1	(-85°)	275.5	(65°)
equatorial	.	293.3	0.319	2.15	313.3	(-85°)	282.9	(-5°)

tropics than it is at present (Fig. 4), although the average temperature of the planet increases to 290.6 K (Table II).

A second reduction in latitudinal temperature gradient derives from more efficient dynamic heat transport as the total atmospheric pressure, P, is raised. At 1.4 AU, $pCO_2 = 2.12$ bars, $P = 3.12$ bars, $c_p = 0.91c_{p_0}$, $m = 1.35m_0$, so, from Eq. (9), $D = 1.56D_0 = 0.91$ W m^{-2} K^{-1}. Figure 4 contrasts the effects of raising the IR opacity of the atmosphere and of enhancing heat transport. The dotted-line profile for Earth at 1.4 AU shows the effect of opacity alone, whereas the solid-line profile for 1.4 AU illustrates the combined influence. Nearly 70% of the reduction in the equator-to-pole temperature gradient between 1.0 AU (47 K) and 1.4 AU (15 K) is caused by the radiative properties of CO_2, while the remainder is caused by dynamics. This is significant because it implies that our results are only weakly sensitive to our uncertain assumptions concerning heat transport in atmospheres vastly different from Earth's.

We next experimented with Earth at 1.4 AU and with a 90° obliquity to illustrate how elevated CO_2 levels affect seasonal temperature cycles. Figure 5 shows that the amplitudes of temperature cycles would be greatly reduced. The reason for this is the same as before: As more CO_2 accumulates in the atmosphere, the global thermal time constant and, hence, global thermal inertia grow. Thus, zonal temperatures respond slowly to changes in insolation, and the magnitudes of the seasonal temperature extremes are reduced.

A comparison of Figs. 5 and 1B shows that the amplitude of the seasonal cycle at +45° latitude is reduced by 30% in moving from 1.0 to 1.4 AU. The 90° obliquity seasonal cycle at 1.4 AU is only slightly greater (2 K) than the observed amplitude for the same latitude on Earth today. Differences in heat capacity and, hence, temperature extremum (315 and 319 K) for the northern and southern poles are shown to be essentially eliminated. We note that Earth would be ice-free in these circumstances and, with the exception of the summertime poles, would be able to support life over an even greater fraction of its surface than it does at present.

Finally, we repeated the geographic variation experiments described in Section 3C with Earth at 1.4 AU to determine if an Earth with a dense CO_2 atmosphere and a supercontinent would be equally habitable. Results from these runs are given in Table II. The promising result is that such a planet would be able to sustain temperatures over a polar supercontinent within the limits of the model to a much higher obliquity (65°) than at 1.0 AU. At 23.5° obliquity, the polar supercontinent would demonstrate a seasonal temperature range comparable to the equator-to-pole gradient for present Earth. This suggests that a wide variety of planets with CO_2-rich atmospheres would be immune to the climatic problems caused by high obliquity.

4. DISCUSSION

An obvious weakness of our model is the averaging of heat capacity, surface albedo, and temperature over 10°-wide latitudinal zones extending around the planet. As mentioned earlier, this causes us to underestimate the amplitude of the seasonal cycle over the continents (except in the supercontinent scenarios, where an entire latitude band may be devoid of water). Also, by averaging the climate parameters around the planet, we have ignored meridional land–sea temperature gradients which affect dynamic heat transport and weather.

Perhaps the most severe limitation of the model is its gross oversimplification of the effects of weather on the global climate. As explained in Section 2D and in the Appendix, we modeled latitudinal heat transport as diffusion, whereas in reality, wind patterns and energy transport are much more complicated. This simplification afforded us speed in computation, but we are not really able to predict how latitudinal energy transport would differ on planets with higher obliquities or with denser atmospheres. Some first-order changes were predicted by adjusting the
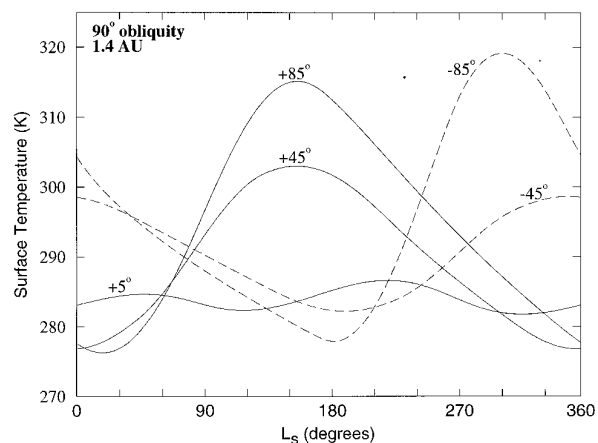

FIG. 5.   Seasonal temperature cycles for Earth at 1.4 AU and with 90° obliquity.

diffusion coefficient, D [Eq. (9)], to account for changes to atmospheric pressure. Large latitudinal temperature gradients in atmospheres of planets at high obliquity (Fig. 1B) may tend to increase heat transport to a greater extent than we predict by driving vigorous Hadley circulation cells and causing increased baroclinic wave activity. We suspect, but cannot prove, that temperature gradients in more realistic dynamic atmospheres would be smaller than predicted here.

A third area of uncertainty is the model's treatment of H_2O clouds, which we assumed to cover exactly half of the planet's surface at all times, as is approximately true on Earth. If H_2O cloud cover increases as the surface temperature warms, as seems likely, then surface temperature extremes may be further buffered by cloud feedback. This is particularly important over polar oceans where the temperatures predicted by our model exceed 320 K at high obliquity. Negative cloud feedback might significantly reduce these summertime extremes, rendering the polar regions much more habitable. A 3-D atmospheric circulation model with predictive clouds is needed to investigate this possibility.

Given the limitations of the present climate model, a natural question is: Why even attempt to study this problem at this crude level of approximation? The answer is that many of our conclusions depend more strongly on atmospheric CO_2 levels and the carbonate–silicate cycle feedback than they do on the details of the atmospheric climate model. The problem deserves to be examined with a 3-D general circulation model, but the results of any such study will be of dubious utility unless it includes the types of feedback processes studied here. Using a 2-D, azimuthally symmetric model (e.g., Farrell 1990) would make the calculation considerably more difficult without improving significantly on such factors as high-latitude heat transport and the spatial distribution of clouds.

5. CONCLUSIONS

Large areas of Earth might not be habitable if its obliquity were as high as 90°. Long periods of darkness and intense sunlight (~90 days at 45° latitude) might be problematic for photosynthetic life. Other forms of life would have to adapt to rapidly varying temperatures (>0.5° K per day) and temperature extremes (>80°C) over the continents. Similar planets, but with smaller continents or with equatorial supercontinents, would have their unfavorably large seasonal cycles damped by the large heat capacity of their oceans. Planets with polar supercontinents would be largely unsuited for land-based life even at modest (e.g., 23.5°) obliquities.

Habitability is less affected by the size or position of continents on planets with dense, CO_2-rich atmospheres. The level of CO_2 is affected by the amount of sunlight a planet receives from its parent star through the carbonate–silicate feedback loop, which should cause pCO_2 to increase with orbital distance. At 1.4 AU, Earth's atmosphere would contain 2.1 bars of CO_2 if the rate of volcanic outgassing remained constant. Aided by the greenhouse effect of its atmosphere, Earth would remain habitable out to distances of 1.40 to 1.46 AU, at which point its surface might be cooled by widespread CO_2 clouds.

A second benefit of a dense CO_2 atmosphere is its high thermal inertia, which limits the seasonal temperature variation and latitudinal temperature gradient for planets at high obliquity. Atmospheres that are dynamically similar to Earth's should have their temperature gradients reduced further by more efficient heat transport as a result of their higher surface pressures. All else being equal (e.g., the size and distribution of continents, H_2O cloud cover, dynamics), most Earth-like planets occupying the outer HZ around their parent stars should be habitable regardless of their obliquity.

APPENDIX: THE ENERGY-BALANCE CLIMATE MODEL

A. Diurnally Averaged Incident Solar Flux (S)

The bolometric solar flux at 1.0 AU, q_0, is 1360 W m^{-2}. The instantaneous solar flux received by a particular latitude is $q_0 \cos Z$, where Z is the solar zenith angle and $\cos Z = \mu$, which is written as

$$\mu = \sin \theta \sin \delta + \cos \theta \cos \delta \cos h. \tag{A1}$$

Here, θ is latitude, δ is solar declination, and h is solar hour angle. Solar declination, δ, depends on obliquity, δ_0, and orbital longitude, L_s, through the equation

$$\sin \delta = -\sin \delta_0 \cos(L_s + \pi/2), \tag{A2}$$

where orbital longitude for circular orbits is a simple function of time t:

$$L_s = \omega t. \tag{A3}$$

In Eq. (A3), ω is the planet's angular velocity, found from Kepler's third law,

$$\omega = 1.721 \times 10^{-20} (GM_\odot)^{1/2} \left(\frac{a}{1.0\,\mathrm{AU}} \right)^{-3/2}, \tag{A4}$$

where G and $M_\odot$ are the gravitational constant and Sun's mass in cgs units, respectively, and a is the planet semimajor axis in AU. The diurnally averaged solar flux is $S = q_0 \bar{\mu}$, and the averaging of μ is over a complete rotation. Averaging first over the sunlit portion of rotation, i.e., over solar hour angle from $h = -H$ to $+H$, where H is the radian half-day length given by

$$\cos H = -\tan \theta \tan \delta, \quad \text{for } 0 < H < \pi, \tag{A5}$$

we obtain

$$\overline{\mu} = \frac{\int_{-H}^{H} dh(\sin\theta\sin\delta + \cos\theta\cos\delta\cos h)}{\int_{-H}^{H} dh} \tag{A6}$$

$$= \left(\sin\theta\sin\delta + \cos\theta\cos\delta\frac{\sin H}{H}\right).$$

Now, the averaging of μ over the entire diurnal cycle is completed by scaling Eq. (A6) by the factor H/π, because $H = \pi$ if the Sun remains above the horizon for a complete rotation. The diurnally averaged solar flux, S, may then be written as

$$S = q_0\left(\frac{H}{\pi}\right)\overline{\mu} \tag{A7}$$

$$= \frac{q_0}{\pi}(H\sin\theta\sin\delta + \cos\theta\cos\delta\sin H),$$

which may be expressed for any planet having an orbital semimajor axis a as

$$S = \frac{q_0}{\pi}\left(\frac{1.0\,\text{AU}}{a}\right)^2 \tag{A8}$$

$$(H\sin\theta\sin\delta + \cos\theta\cos\delta\sin H).$$

B. Top-of-Atmosphere Albedo (A)

The fraction of short-wave solar energy returned to space as a consequence of atmospheric or surface scattering is the top-of-atmosphere (TOA) albedo. TOA albedo depends both on the distance photons travel through the atmosphere, which is set by the solar zenith angle, and on the surface albedo. Levels of CO_2 and H_2O affect TOA albedo by their respective contributions to Rayleigh scattering and absorption. CO_2 raises the albedo significantly because its cross section for Rayleigh scattering is more than 2.5 times that of nitrogen. H_2O is an efficient Rayleigh scatterer, but it is also a good absorber in the near IR. Hence, for the low temperatures and small H_2O mixing ratios encountered by our model, the dominant effect of H_2O is to decrease albedo by raising atmospheric absorption. The water vapor contribution to Rayleigh scattering does not begin to dominate its contribution to absorption until surface temperatures exceed ~ 360 K, and the stratospheric H_2O mixing ratio becomes large (Kasting 1988).

Following Caldeira and Kasting (1992), we parameterized TOA albedo as a second-order polynomial of four variables: pCO_2 (here referred to as p), μ, surface temperature, T, and surface albedo, a_s. We obtained best fits to the results of more than 24,000 runs of the radiative–convective climate model used by Kasting and Ackerman (1986) and Kasting (1988, 1991). We divided model output in half at a temperature $T = 280$ K to yield smaller rms errors than was possible with one fit over the entire temperature range (190 K $< T <$ 360 K). The fits we obtained may be applied confidently for 10^{-5} bar $< p <$ 10 bars, $0 < a_s < 1$, and $0 < \mu < 1$.

For 190 K $< T <$ 280 K,

$$A = -6.8910 \times 10^{-1} + 1.0460a_s + 7.8054 \times 10^{-3}T - 2.8373$$

$$\times 10^{-3}p - 2.8899 \times 10^{-1}\mu - 3.7412 \times 10^{-2}a_sp$$

$$- 6.3499 \times 10^{-3}\mu p + 2.0122 \times 10^{-1}a_s\mu - 1.8508$$

$$\times 10^{-3}a_sT + 1.3649 \times 10^{-4}\mu T + 9.8581 \times 10^{-5}pT$$

$$+ 7.3239 \times 10^{-2}a_s^2 - 1.6555 \times 10^{-5}T^2 + 6.5817$$

$$\times 10^{-4}p^2 + 8.1218 \times 10^{-2}\mu^2, \tag{A9}$$

and for 280 K $< T <$ 370 K,

$$A = 1.1082 + 1.5172a_s - 5.7993 \times 10^{-3}T + 1.9705 \times 10^{-2}p$$

$$- 1.8670 \times 10^{-1}\mu - 3.1355 \times 10^{-2}a_sp - 1.0214$$

$$\times 10^{-2}\mu p + 2.0986 \times 10^{-1}a_s\mu - 3.7098 \times 10^{-3}a_sT$$

$$- 1.1335 \times 10^{-4}\mu T + 5.3714 \times 10^{-5}pT + 7.5887$$

$$\times 10^{-2}a_s^2 + 9.2690 \times 10^{-6}T^2 - 4.1327 \times 10^{-4}p^2$$

$$+ 6.3298 \times 10^{-2}\mu^2. \tag{A10}$$

The rms errors for the fits are 7.58 and 4.66 W m^{-2}, respectively, when scaled by the planetary-average incident solar flux ($q_0/4$). The fits were obtained assuming an isothermal stratosphere (as in Kasting 1991) and a troposphere that is fully saturated with H_2O vapor.

One should note that there is a discrepancy between Eqs. (A9) and (A10) above and their analog equation, Eq. 5, of Caldeira and Kasting (1992). An analysis of these formulas reveals that TOA albedo increases with Z in Eqs. (A9) and (A10) above, as it should, but decreases with Z in the older Eq. 5. The inconsistency originated with differences in the way the radiative–convective model, which was used to make both sets of fits, was used to calculate stratospheric temperature, T_{strat}. Caldeira and Kasting calculated T_{strat} using Eq. 1 of Kasting (1991),

$$T_{strat} = \frac{1}{2^{1/4}}\left[\frac{S}{4\sigma}(1 - A)\right]^{1/4}, \tag{A11}$$

where S is incident solar flux, and σ is the Stefan–Boltzmann constant. This equation, however, is appropriate only for global-average conditions (i.e., for $Z = 60°$) and, thus, was applied incorrectly in calculating T_{strat} and TOA albedo for latitudes having solar zenith angles different from this value. We circumvented this problem by parameterizing T_{strat} as the following function of Z:

$$T_{strat}(Z) = T_{strat}(60°)\left[\frac{F_s(Z)}{F_s(60°)}\right]^{1/4}. \tag{A12}$$

Here, in the notation of Kasting (1991), F_s is the absorbed fraction of incident solar flux, which was calculated for a variety of zenith angles between 0° and 90° using the radiative–convective model, and $T_{strat}(60°)$ was obtained using Eq. (A11) as before.

C. Surface Albedo (a_s)

Zonal area was partitioned between ocean and continents for the three geographic cases given in Table III. Zonal land–sea fractions for present Earth were taken from Sellers (1965). Surface albedo depends on temperature through its effect on the extent and reflectance properties of snow and ice cover. We assigned albedos to land and oceanic surfaces for three different temperature regimes.

For $T > 273$ K, land was assigned an albedo of 0.20, which is characteristic of many terrestrial surfaces (Kondrat'ev 1969). The albedo of unfrozen ocean depends on solar zenith angle through the Fresnel reflectance formulas for water and can range from 0 to 100%. The fraction of incident short-wave energy reflected from a smooth oceanic surface ($n = 1.33$), for $0° < Z < 90°$, was read from a table prepared by Kondrat'ev (1969, p. 439).

For 263 K $< T <$ 273 K, land was allowed an unstable snow cover having an albedo of 0.45, and sea-ice with $a_s = 0.55$ was permitted to form in the oceans. We used data from Table 1 of Thompson and Barron (1981) to parameterize the ocean fraction covered by sea ice, f_i, as a function of surface temperature,

$$f_i = 1 - e^{(T-273\,\text{K})/10}. \tag{A13}$$

TABLE III
Latitudinal Land–Sea Fractions for Three Model Geographies

	Ocean fraction		
Latitude	Present geog.	Equatorial geog.	Polar geog.
90—80N	0.934	1.000	1.000
80—70	0.713	1.000	1.000
70—60	0.294	1.000	1.000
60—50	0.428	1.000	1.000
50—40	0.475	1.000	1.000
40—30	0.572	1.000	1.000
30—20	0.624	1.000	1.000
20—10	0.736	0.250	1.000
10—0	0.772	0.000	1.000
0—10S	0.764	0.000	1.000
10—20	0.780	0.250	1.000
20—30	0.769	1.000	0.367
30—40	0.888	1.000	0.000
40—50	0.970	1.000	0.000
50—60	0.992	1.000	0.000
60—70	0.896	1.000	0.000
70—80	0.246	1.000	0.000
80—90	0.000	1.000	0.000

For $T < 263$ K, the continents and oceans were assigned an albedo of 0.7, which is appropriate for stable snow cover over an ice cap.

The contribution of H_2O clouds to the global albedo was treated simply by assuming that clouds cover 50% of the surface at all times and that the albedo of the cloud cover depends linearly on solar zenith angle (Cess 1976):

$$a_s = \alpha + \beta Z. \tag{A14}$$

The values of α (-0.078) and β (0.65) were adjusted to allow the model to reproduce Earth's latitudinal albedo profile (Jacobowitz et al. 1979). If we delineate albedos and zonal surface fractions for ocean, land, and ice using subscripts o, l, and i respectively, the zonally averaged surface albedo a_s may be expressed as

$$a_s = 0.5\{(1 - f_o)a_l + f_o[f_i a_i + (1 - f_i)a_o]\} + 0.5(\alpha + \beta Z). \tag{A15}$$

D. Effective Heat Capacity (C)

The thermal time scale, τ, depends on the effective zonal heat capacity, C, through the equation

$$\tau = \frac{CT}{I}, \tag{A16}$$

where I is the outgoing infrared flux and $C = \rho c_p \Delta l$. Over the continents, ρ, c_p, and Δl are the density, heat capacity, and depth of the atmosphere, giving $\tau \sim 50$ days. Oceanic areas have much longer thermal time scales ($\tau \sim 5$ years) because the surface temperature is coupled to the slowly varying temperature of the wind-mixed ocean layer with $\Delta l = 50$ to 100 m. We adopted the effective heat capacity of the atmosphere over land, C_1, used by North et al.. (1983), 5.25×10^6 J m^{-2} K^{-1}. The effective heat capacities of the atmosphere over ocean, C_0, and sea-ice, C_i, depend in an unpredictable way on atmospheric and oceanic dynamics and, hence, can be treated as free parameters in time-dependent EBCMs.

North et al. (1983) chose $C_o = 60C_1$ and $C_i = 9.2C_1$, where the value of C_o corresponds to a wind-mixed ocean layer 75 m deep, and the value of C_i was introduced and adjusted to raise the amplitudes of seasonal cycles in the high latitudes. We required a similar, albeit slightly more complicated, approach to reduce τ over the poles. We introduced an additional frozen oceanic heat capacity to resolve expected thermal differences between surfaces of thin transient sea-ice (263 K $< T <$ 273 K) and of a stable ice cap ($T < 263$ K). In the first temperature regime, we allowed $C_i = 9.2C_1$, and over the ice cap, $C_i = 2.0C_1$. We also reduced the depth of our wind-mixed ocean layer to 50 m, giving $C_o = 40C_1$, to better match the observed latitudinal distribution of seasonal cycle amplitudes (North and Coakley 1979). We obtained a zonally averaged effective heat capacity using the equation

$$C = (1 - f_o)C_1 + f_o\{(1 - f_i)C_o + f_iC_i\}. \tag{A17}$$

To summarize, the values of surface albedo and effective heat capacity used in the model are given in Table IV.

E. Outgoing Infrared Flux (I)

As was done for TOA albedo, we used the radiative–convective model developed by Kasting to parameterize long-wave energy lossess to space as a function of T and pCO_2 (p). Surface temperature sets the humidity and, hence, the contribution of H_2O vapor to the greenhouse effect. The parameterized outgoing IR flux is a polynomial fit to output from $\sim$300 runs of the radiative–convective model.

Because we sought a numerical, rathere than analytic, solution to the energy-balance equation, Eq. (1), we did not require the form of I to be the simple linear function of T (e.g., $A + BT$) used in similar models (Caldeira and Kasting 1992, North et al. 1981). We thereby used a higher-order polynomial in T to obtain a low rms error (4.56 W m^{-2}) over a larger range (190 K $< T <$ 380 K) of temperatures than obtained by Caldeira and Kasting (Eqs. 2-4). The polynomial given below may be applied in the range $10^{-5} < p < 10$ bars.

$$\begin{aligned}
I = {} & 9.468980 - 7.714727 \times 10^{-5}\phi - 2.794778T - 3.244753 \\
& \times 10^{-3}\phi T - 3.547406 \times 10^{-4}\phi^2 + 2.212108 \times 10^{-2}T^2 \\
& + 2.229142 \times 10^{-3}\phi^2 T + 3.088497 \times 10^{-5}\phi T^2 \\
& - 2.789815 \times 10^{-5}\phi^2 T^2 - 3.442973 \times 10^{-3}\phi^3 - 3.361939 \\
& \times 10^{-5}T^3 + 9.173169 \times 10^{-3}\phi^3 T - 7.775195 \\
& \times 10^{-5}\phi^3 T^2 - 1.679112 \times 10^{-7}\phi T^3 + 6.590999 \\
& \times 10^{-8}\phi^2 T^3 + 1.528125 \times 10^{-7}\phi^3 T^3 - 3.367567 \times 10^{-2}\phi^4 \\
& - 1.631909 \times 10^{-4}\phi^4 T + 3.663871 \times 10^{-6}\phi^4 T^2 \\
& - 9.255646 \times 10^{-9}\phi^4 T^3. \tag{A18}
\end{aligned}$$

TABLE IV
Model Surface Albedo and Heat Capacity

	Ocean		Land	
Temperatures (K)	a_s	C/C_1	a_s	C/C_1
$T > 273$	0 - 0.99	40.0	0.2	1
$263 < T < 273$	0.55	9.2	0.45	.
$T < 263$	0.7	2.0	0.7	.

Note: a_s is surface albedo, and C is effective heat capacity (C_1 for land).

Here, $\phi = \log_e(p/3.3 \times 10^{-4})$. As with the albedo fit, the troposphere was assumed to be fully saturated with H_2O and the stratosphere was isothermal. Reduction in the outgoing IR flux by H_2O-cloud absorption was taken into account by subtracting 14.06 W m^{-2} from Eq. (A18). The value of the cloud correction was determined by requiring the model to obtain Earth's observed globablly averaged surface temperature (288 K) for the observed globally averaged TOA albedo (0.31).

F. CO$_2$ Clouds

The troposphere for each zone was searched for the presence of CO_2 clouds using the following assumptions and procedures. The depth of the troposphere was determined by our assumptions regarding stratospheric temperature. We parameterized T_{strat} as a function of pCO_2 and T, in the same way we performed the fit to I to obtain Eq. (A18). We obtained

$$T_{strat} = -188.1 - 1.955\phi + 3.810\phi^2 + 2.328T + 3.733$$
$$\times 10^{-4}\phi T - 2.856 \times 10^{-2}\phi^2 T - 3.329 \times 10^{-3}T^2$$
$$+ 2.214 \times 10^{-5}\phi T^2 + 4.605 \times 10^{-5}\phi^2 T^2, \qquad (A19)$$

where ϕ is the same as before. The fit was performed with $Z = 60°$ using Eq. (A11), which means that we slightly overestimated T_{strat}, and hence tropospheric depth, at the poles while underestimating their values at the equator. This suggests that clouds in reality are less likely to form at the poles and more likely to form at the equator than the model indicates. The effect of this error on our results, however, is expected to be small because a counterbalancing error is introduced in approximating tropospheric lapse rate, as will be discussed below.

Once T_{strat} was found, the troposphere was divided into 20 layers of equal thickness. The model stepped from the surface to the tropopause by assuming a constant lapse rate $c = 6.5$ K km^{-1} and the barometric law for CO_2:

$$p(h) = p(0)\left(\frac{T(h)}{T(0)}\right)^{mg/kc}. \qquad (A20)$$

Here, g is the gravitational constant, k is the Boltzmann constant, h is physical height, and, here, m is the mean molecular weight of the atmosphere. Our assumed lapse rate for this calculation is slightly smaller than over the poles (~ 10 K km^{-1}) and slightly larger than over the tropics (3–4 K km^{-1}) in reality, and so, here, we underestimated polar cloud cover while overestimating clouds in the tropics. Thus, we err in the opposite sense of our previous error introduced in approximating T_{strat}, which should mitigate the effects of both approximations for this calculation. Clouds form at a height at which $p > p_{sat}$, the saturation vapor pressure, which we calculated using Eqs. A5 and A6 of Kasting (1991). Finally, we determined the fraction of the globe that is covered with CO_2 clouds by summing over the latitudes in which clouds form and weighting them by zonal area and insolation.

G. Solving the Model

We obtained latitudinal temperature profiles by finding numerical solutions to the zonal energy-balance equation, Eq. (1), with the constraint that the profiles also be solutions to the CO_2 weathering-balance equation, Eq. (3). We integrated both equations simultaneously using the following method. We began with an isothermal planet (e.g., $T = 288$ K) at the vernal equinox ($L_s = 0$), and stepped the planet in its orbit by incrementing the time ($10^4 < \Delta t < 8.64 \times 10^4$ sec) and orbit longitude using Eq. (A3).

For each Δt, we performed a spatial integration over all latitude zones. Orbital longitude set the solar declination according to Eq. (A2) and, hence, the diurnally averaged insolation for each zone using Eq. (A8).

The TOA albedo, outgoing IR flux, and weathering rate, which all depend on surface temperature, followed from Eqs. (A9)/(A10), (A18), and (3), respectively. The dynamic heat transport term of Eq. (1) was spatially differenced to second order in x, and operated on the global latitudinal temperature profile. The pressure-dependent transport coefficient D was calculated using Eq. (9). Once the climate parameters for each zone were computed, the first term of Eq. (1) was temporally differenced according to our assumptions made concerning effective heat capacity, and the surface temperatures were updated.

Every five orbits, we compared the seasonal-global mean weathering rate to the rate of CO_2 production by volcanos, and if the ratio of weathering to outgassing was less than unity, we increased pCO_2. Conversely, we decreased pCO_2 for ratios greater than unity. The size of the adjustment was proportional to the size of the rate imbalance. We staggered the adjustments to pCO_2 by five orbital periods to allow the slowly varying temperature of the oceans time to respond. We iterated on this procedure until the weathering rate converged to within 10^{-3} of the outgassing rate.

The rate of convergence was affected predominantly by semimajor axis, which set the orbital period, by the step size Δt, and by the initial choice for pCO_2. For $a = 1.0$ AU, $\Delta t = 8.64 \times 10^4$ sec, and $p_0 = 330$ ppm, the model calculations required 38 sec of CPU time on a CRAY supercomputer. By contrast, convergence took 59 sec for the same time step, but with $a = 1.4$ AU, and $p_0 = 2.0$ bars.

REFERENCES

Berner, R. A., A. C. Lasaga, and R. M. Garrels 1983. The carbonate–silicate geochemical cycle and its effect on atmospheric carbon dioxide over the past 100 million years. *Am. J. Sci.* **283,** 641–683.

Butler, R. P., and G. W. Marcy 1996. A planet orbiting 47 Ursae Majoris. *Astrophys. J.* **464,** L153–L156.

Butler, R. P., G. W. Marcy, E. Williams, H. Hauser, and P. Shirts 1996. Three new "51 Peg-type" planets. *Astrophys. J.*, submitted.

Caldeira, K., and J. F. Kasting 1992. Susceptibility of early Earth to irreversible glaciation caused by carbon dioxide clouds. *Nature* **359,** 226–228.

Cess, R. D. 1976. Climatic change: An appraisal of atmospheric feedback mechanisms employing zonal climatology. *J. Atmos. Sci.* **33,** 1831–1843.

Cochran, W. D., A. P. Hatzes, R. P. Butler, and G. W. Marcy 1996. The discovery of a planetary companion to 16 Cygni B. *Astrophys. J.*, submitted.

Farrell, B. F. 1990. Equable climate dynamics. *J. Atmos. Sci.* **47,** 2986–2995.

Gatewood, G. 1996. Lalande 21185. *Bull. Am. Astron. Soc.* **28,** 885.

Gierasch, P. J., and O. B. Toon 1973. Atmospheric pressure variation and the climate of Mars. *J. Atmos. Sci.* **30,** 1502–1508.

Hartmann, W. K., R. J. Phillips, and G. J. Taylor 1986. *Origin of the Moon.* Lunar and Planetary Inst., Houston.

Hoffert, M. I., A. J. Callegari, C. T. Hsiech, and W. Ziegler 1981. Liquid water on Mars: An energy balance climate model for CO_2/H_2O atmospheres. *Icarus* **47,** 112–129.

Holland, H. D. 1978. *The Chemistry of the Atmosphere and Oceans.* Wiley, New York.

Jacobowitz, H., W. L. Smith, H. B. Howell, F. W. Nagle, and J. R. Hickery

1979. The first 18 months of planetary radiation budget measurements from Nimbus 6 ERB experiment. *J. Atmos. Sci.* **36,** 501–507.

Kasting, J. F. 1988. Runaway and moist greenhouse atmospheres and the evolution of Earth and Venus. *Icarus* **74,** 472–494.

Kasting, J. F. 1991. CO_2 condensation and the climate of early Mars. *Icarus* **94,** 1–13.

Kasting, J. F., and T. P. Ackerman 1986. Climatic consequences of very high carbon dioxide levels in the Earth's early atmosphere. *Science* **234,** 1383–1385.

Kasting, J. F., D. P. Whitmire, and R. T. Reynolds 1993. Habitable zones around main sequence stars. *Icarus* **101,** 108–128.

Kondrat'ev, K. Y. A. 1969. Albedo of the underlying surface and clouds. In *Radiation in the Atmosphere* (K. Y. A. Kondrat'ev, Ed.), pp. 411–452. Academic Press, New York.

Laskar, J., and P. Robutel 1993. The chaotic obliquity of the planets. *Nature* **361,** 608–614.

Laskar, J., F. Joutel, and P. Robutel 1993. Stabilization of the Earth's obliquity by the Moon. *Nature* **361,** 615–617.

Lindzen, R. S., and B. Farrell 1977. Some realistic modifications of simple climate models. *J. Atmos. Sci.* **34,** 1487–1501.

Marcy, G. W., and R. P. Butler 1996. A planetary companion to 70 Virginis. *Astrophys. J.* **464,** L147–L151.

Marshall, H. G., J. C. G. Walker, and W. R. Kuhn 1988. Long-term climate change and the geochemical cycle of carbon. *J. Geophys. Res.* **93,** 791–801.

Mayor, M., and D. Queloz 1995. A Jupiter-mass companion to a solar-type star. *Nature* **378,** 355–359.

North, G. R., and J. A. Coakley 1979. Differences between seasonal and mean annual energy balance model calculations of climate and climate sensitivity. *J. Atmos. Sci.* **36,** 1189–1203.

North, G. R., R. F. Cahalan, and J. A. Coakley 1981. Energy balance climate models. *Rev. Geophys. Space Phys.* **19,** 91–121.

North, G. R., J. G. Mengel, and D. A. Short 1983. Simple energy balance model resolving the seasons and the continents: Application to the astronomical theory of the ice ages. *J. Geophys. Res.* **88,** 6576–6586.

Pollack, J. B., J. F. Kasting, S. M. Richardson, and K. Poliakoff 1987. The case for a wet, warm climate on early Mars. *Icarus* **71,** 203–224.

Schubert, G. 1983. General circulation and the dynamical state of the Venus atmosphere. In *Venus* (D. M. Hunten, L. Colin, T. M. Donahue, and V. I. Moroz, Eds.), pp. 681–765. Univ. of Arizona Press, Tucson.

Segerer, A. H., S. Burggraf, G. Fiala, G. Huber, R. Huber, and K. O. Stetter 1993. Life in hot springs and hydrothermal vents. *Origins Life* **23,** 77–90.

Sellers, W. D. 1965. *Physical Climatology.* Univ. of Chicago Press, London.

Stone, P. H. 1972. A simplified radiative–dynamical model for the static stability of rotating atmospheres. *J. Atmos. Sci.* **29,** 405–417.

Thompson, S. L., and E. J. Barron 1981. Comparison of Cretaceous and present Earth albedos: Implications for the causes of paleoclimates. *J. Geol.* **89,** 143–167.

Touma, J., and J. Wisdom 1993. The chaotic obliquity of Mars. *Science* **259,** 1294–1297.

Walker, J. C. G., P. B. Hays, and J. F. Kasting 1981. A negative feedback mechanism for the long-term stabilization of Earth's surface temperature. *J. Geophys. Res.* **86,** 9776–9782.

Ward, W. R. 1973. Large scale variations in the obliquity of Mars. *Science* **181,** 260–262.

Ward, W. R. 1974. Climatic variations on Mars: I. Astronomical theory of insolation. *J. Geophys. Res.* **79,** 3375–3386.

Ward, W. R. 1979. Present obliquity oscillations of Mars: Fourth-order accuracy in orbital *e* and *i J. Geophys. Res.* **84,** 237–241.

Ward, W. R. 1991. Resonant obliquity of Mars? *Icarus* **94,** 160–164.

Wetherill, G. W. 1996. The formation and habitability of extra-solar planets *Icarus* **119,** 219–238.

Williams, D. M., J. F. Kasting, and K. Caldeira 1996. Chaotic obliquity variations and planetary habitability. In *Circumstellar Habitable Zones—Proceedings of the First International Conference* (L. Doyle, Ed.), pp. 43–62. Travis House, Menlo Park, CA.

Williams, D. M., J. F. Kasting, and R. A. Wade 1997. Habitable moons around extrasolar giant planets. *Nature* **385,** 234–236.

Wolszczan, A. 1994. Confirmation of Earth-mass planets orbiting the millisecond pulsar PSR B1257 + 12. *Science* **264,** 538–542.